

# A Conformal Thin-Sandwich Solver for Generic Initial Data

William E. East<sup>1</sup>, Fethi M. Ramazanoğlu<sup>1</sup>, and Frans Pretorius<sup>1</sup>

<sup>1</sup>*Department of Physics, Princeton University,  
Princeton, NJ 08544, USA.*

We present a new scheme for constructing initial data for the Einstein field equations using the conformal thin-sandwich formulation that does not assume conformal flatness or approximate Killing vectors. This includes a method for determining free data based on superposition, as well as a way to handle black hole singularities without excision. We numerically solve the constraint equations using a multigrid algorithm with mesh refinement. We demonstrate the efficacy of the method with initial data solutions for several applications: a quasi-circular binary black hole merger, a dynamical capture black hole-neutron star merger, and an ultrarelativistic collision.

## I. INTRODUCTION

The purview of numerical relativity has extended to include not only relativity theory, but a wide range of other topics. Motivated by current and upcoming efforts to detect gravitational waves [1–5], there has been extensive work on mergers of binary compact objects (BCOs) [6] including binary black holes (BH-BH) [7–9], binary neutron stars (NS-NS) [10] and black hole-neutron star (BH-NS) systems [11, 12]. In addition to binaries in quasi-circular orbits there has also been recent studies of eccentric binaries as may arise from dynamical capture [13–15]. Other work of interest to astrophysics include gravitational collapse of stars [16, 17], black hole accretion [18], and the nature of cosmological singularities [19, 20]. Aside from astrophysical systems, numerical relativity has also emerged as a useful tool to explore various concepts in gravity and high energy physics [21], such as critical collapse [22], ultrarelativistic collisions [23–27], the gauge/gravity duality [28–32], gravity and black holes in higher dimensions [33–35], and the (in)stability of Anti de-Sitter spacetime [36]. In all these applications, a necessary ingredient is a good method for constructing initial data (ID). Here we present a new initial data solver, based on the conformal thin-sandwich (CTS) [37] formulation, which we have designed to be more generally applicable to a range of physical scenarios by avoiding symmetry or simplifying assumptions.

There has been extensive research on the problem of constructing ID for general relativity and detailed reviews can be found in [38–41]. Early attempts at solving the initial data problem relied on certain assumptions to make the mathematical formulation of the problem more tractable, such as conformal flatness and maximal slicing. The widely used Bowen-York solution [42] is one such example. These assumptions are restrictive since, for example, the isolated Kerr black hole does not admit conformally flat slices [43] and consequently the Bowen-York solution cannot be used to construct black holes with spin higher than  $S/M_{ADM}^2 = 0.928$  [44]. Other examples include the use of quasi-equilibrium assumptions for constructing ID for binary systems (such as approximate helical Killing vectors or the like, and approximate

hydrostatic equilibrium for any matter in the system); see for example [45–60]. This serves as a good approximation for astrophysically motivated quasi-circular inspiral sufficiently far from merger, though is not valid for eccentric mergers or the ultrarelativistic scattering problem. Many of these studies made further simplifying assumptions, such as conformal flatness, which does not have an astrophysical motivation. Attempts to supply more realistic conformal initial data include superposition of isolated black hole spacetimes [61–65], and in addition using post-Newtonian solutions [66, 67] and matched asymptotic expansions to supply an initial outgoing radiation field [68–70]. Using superposed data allowed evolution of binary black holes in quasi-circular orbits with spins exceeding the Bowen-York limit [71]. A further alternative approach, initially applied to binaries including neutron stars, involves solving the full Einstein-Euler system of equations with a waveless and/or near-zone helical symmetry approximation [59, 72–74].

Since our goal is to have a more general purpose numerical initial data solver that can be used for a range of applications, as outlined in the first paragraph, we will use the CTS formalism with arbitrary conformal metric and other free data to be chosen as needed for the particular application. For our first version of the code, as presented here, we restrict to four-dimensional, asymptotically-flat spacetimes, with application to BCO interactions. For the free data we use superposed, boosted single CO spacetimes. At large separation this is a good approximation for the physical metric of dynamical capture binaries and the ultrarelativistic scattering problem, and the non-linear corrections from solving the CTS equations are small. For quasi-circular binaries, again at large separation this is a good approximation. However, unlike the scattering problems, at practical (due to limited computational resources) initial separations to allow evolution through merger, the simple superposition we use at present will not give improved astrophysically relevant ID compared to current quasi-equilibrium approaches. Compared to existing studies using superposed data, what is novel about our work is the inclusion of matter to also model CO fluid “stars,” and the consideration of ultrarelativistic initial boosts with Lorentz factors up to 10.

Another novel aspect of this work is how we handle black hole singularities. Most existing approaches either use some form of boundary condition on a trapped surface on or inside each black hole (see for example [40, 50, 75]), or use a slice that maps the interior region of the computational domain for each black hole to either part (so called “trumpets” [76]) or all (“punctures” [77]) of a different asymptotically flat region spanned by an Einstein-Rosen Bridge (for a novel variant that does not require separation of the metric into a background piece and conformal factor see [78]). Here we follow an alternative approach where some distance inside the apparent horizon of each black hole we replace the vacuum interior with an (unphysical) distribution of stress-energy to regularize the interior metric. This is similar to the “turduckening” evolution scheme [79, 80]. However, since we use excision to subsequently evolve the initial data, with the excision surface chosen to entirely contain the unphysical matter, here it is merely a device to set up a simple initial data problem without explicit interior boundary conditions or singularities. Note however that if we were to solve the ID on a domain with traditional excision surfaces inside each black hole, we would (assuming a well-posed elliptic problem) obtain the same solution exterior with appropriate excision boundary conditions, though the mapping between some unphysical interior and appropriate boundary conditions would be non-trivial and in general non-unique.

An outline of the rest of the paper is as follows. In Sec. II we review the CTS formulation, describe our method for choosing the metric and fluid free data, outline the scheme for regularizing black hole solutions, and describe how we numerically solve the constraint equations using a multigrid solver. In Sec. III we present examples of initial data obtained with our solver for quasi-circular, eccentric, and ultrarelativistic mergers of compact objects. Finally, we comment on our results and discuss possible future improvements in Sec. IV. In the Appendix we give some details on how we treat mesh refinement boundaries in our multigrid algorithm. We use geometric units where Newton’s constant  $G = 1$  and the speed of light  $c = 1$ .

## II. COMPUTATIONAL METHODOLOGY

### A. Conformal thin-sandwich equations

To formulate the initial data problem for general relativity, we start by foliating spacetime with a family of spacelike hypersurfaces  $\Sigma_t$  parametrized by  $t$ . The normal vector to these surfaces  $n^\mu$  and the generator of time translations  $t^\mu$  satisfy

$$t^\mu = \alpha n^\mu + \beta^\mu \quad (1)$$

where  $\alpha$  is the lapse and  $\beta^\mu$  is the shift, which is tangent to  $\Sigma_t$  ( $n_\mu \beta^\mu = 0$ ). We use the standard convention

where Greek indices run through  $\{0, 1, 2, 3\}$  and represent the full spacetime coordinates, while Latin indices run through  $\{1, 2, 3\}$  and represent coordinates intrinsic to a given spatial hypersurface. Using the orthogonal projection operator  $\perp^\mu{}_\nu \equiv \delta^\mu{}_\nu + n^\mu n_\nu$ , we obtain the induced metric on  $\Sigma_t$ ,  $\gamma_{ij} \equiv g_{\mu\nu} \perp^\mu{}_i \perp^\nu{}_j$ , where  $g_{\mu\nu}$  is four-dimensional spacetime metric. The line element can be written in terms of these quantities as

$$ds^2 = -\alpha^2 dt^2 + \gamma_{ij}(dx^i + \beta^i dt)(dx^j + \beta^j dt). \quad (2)$$

The extrinsic curvature of a slice  $\Sigma_t$  can be written in terms of a Lie derivative as

$$K_{ij} \equiv -\frac{1}{2} \mathcal{L}_n \gamma_{ij}. \quad (3)$$

Projecting the Einstein equations onto the hypersurface  $\Sigma_t$  one obtains the constraint equations

$$R + K^2 + K_{ij}K^{ij} = 16\pi E, \quad (4)$$

$$D_j K^{ij} - D^i K = 8\pi p^i, \quad (5)$$

where  $K = \gamma^{ij}K_{ij}$ ,  $R$  and  $D_i$  are the Ricci scalar and covariant derivative associated with  $\gamma_{ij}$ , respectively, and  $E$  and  $p^i$  are the energy and momentum density as measured by an Eulerian observer, respectively.

In the language of the 3+1 decomposition, initial data for the Einstein field equations (and any matter evolution equations) are a set of 20 functions representing the components of  $\alpha, \beta^i, \gamma_{ij}, K_{ij}, E$  and  $p^i$  on the initial slice  $\Sigma_t$  that together satisfy the constraints (4-5). Though, in principle, there are numerous conceivable ways of coming up with consistent initial data, it is challenging to separate freely-specifiable versus constrained degrees of freedom in a manner where the underlying physical interpretation of the free data is transparent, and where the choice of the free data leads to a well-posed set of constraint equations. The CTS method [37] is a prescription for this separation of degrees of freedom that begins with a conformal decomposition of the spatial metric and the extrinsic curvature. Introducing the conformal factor  $\Psi$  we define

$$\tilde{\gamma}_{ij} \equiv \Psi^{-4} \gamma_{ij}, \quad (6)$$

$$\begin{aligned} \hat{A}^{ij} &\equiv \Psi^{10} \left( K^{ij} - \frac{1}{3} K \gamma^{ij} \right) \\ &= \frac{1}{2\tilde{\alpha}} \left[ \dot{\tilde{\gamma}}^{ij} + \tilde{D}^i \beta^j + \tilde{D}^j \beta^i - \frac{2}{3} \tilde{\gamma}^{ij} \tilde{D}_k \beta^k \right], \end{aligned} \quad (7)$$

where  $\dot{\tilde{\gamma}}^{ij} \equiv \Psi^4 (\dot{\gamma}^{ij} - \frac{1}{3} \gamma^{ij} \gamma_{kl} \dot{\gamma}^{kl})$  is defined to be traceless, the overdot indicates a time-derivative,  $\tilde{\alpha} \equiv \Psi^{-6} \alpha$ , and  $\tilde{R}$  and  $\tilde{D}_i$  are the Ricci scalar and covariant derivative associated with  $\tilde{\gamma}_{ij}$ , respectively. With these definitions we can rewrite (4) and (5) in the CTS form as

$$\tilde{D}_i \tilde{D}^i \Psi - \frac{\tilde{R}}{8} \Psi + \frac{1}{8} \hat{A}_{ij} \hat{A}^{ij} \Psi^{-7} - \frac{K^2}{12} \Psi^5 = -2\pi \Psi^{-3} \tilde{E} \quad (8)$$

$$\tilde{D}_j \hat{A}^{ij} - \frac{2}{3} \Psi^6 \tilde{D}^i K = 8\pi \tilde{p}^i \quad (9)$$

with  $\tilde{p}^i \equiv \Psi^{10} p^i$ ,  $\tilde{E} \equiv \Psi^8 E$ . Initial data is obtained by solving this system of four elliptic equations for  $\Psi$  and  $\beta^i$  (upon substitution of (7) into (9)), where  $\tilde{\gamma}_{ij}$ ,  $\dot{\tilde{\gamma}}^{ij}$ ,  $K$ ,  $\tilde{\alpha}$ ,  $\tilde{E}$ , and  $\tilde{p}^i$  are the “free data” which can be freely specified to reflect the physical system under investigation.

### B. Superposed free data

Under the conformal thin-sandwich method one is free to choose any values for  $\tilde{\gamma}_{ij}$ ,  $\dot{\tilde{\gamma}}^{ij}$ ,  $\tilde{\alpha}$ ,  $K$ ,  $\tilde{E}$ , and  $\tilde{p}^i$  for which a solution can be found. In this section we outline our method for determining this free data in order to construct initial data representing binary systems. The basic idea is as follows. Since solutions to the Einstein equations representing isolated compact objects (black holes, stars, etc.) are well known, and since if the separation between the objects is not too small the solution describing two compact objects is well-approximated by superposing the two isolated solutions, we therefore set our free data using such a superposed solution and then solve the constraint equations in order to obtain the non-linear correction.

There are many ways to combine the metrics representing isolated compact objects. The method we use is based on the 3 + 1 splitting. Let  $\gamma_{ij}^{(1)}$ ,  $\dot{\gamma}_{ij}^{(1)}$ ,  $\alpha^{(1)}$ , and  $\beta^{i(1)}$  represent the spatial metric, time derivative of the spatial metric, lapse, and shift, respectively, of the first isolated solution (e.g. a boosted black hole or neutron star solution) and similarly for the second isolated solution. Then, we construct the following quantities:

$$\gamma_{ij}^{(\text{sup})} = \gamma_{ij}^{(1)} + \gamma_{ij}^{(2)} - f_{ij} \quad (10)$$

$$\dot{\gamma}_{ij}^{(\text{sup})} = \dot{\gamma}_{ij}^{(1)} + \dot{\gamma}_{ij}^{(2)} \quad (11)$$

$$\alpha^{(\text{sup})} = \alpha^{(1)} + \alpha^{(2)} - 1 \quad (12)$$

$$\beta^{i(\text{sup})} = \beta^{i(1)} + \beta^{i(2)} \quad (13)$$

where  $f_{ij}$  is the flatspace metric. This particular construction will break down if  $\alpha^{(\text{sup})} \leq 0$  or  $\det[\gamma_{ij}^{(\text{sup})}] \leq 0$  anywhere in the domain, which would then require some other way of combining the metrics, for example, using distance-weighted attenuation functions as in [81]. (In [62] it was also found necessary to enforce a desired asymptotic fall off of the superposed metric, due to the use of a co-rotating frame.) However, these conditions are not violated for the cases considered here. From the above quantities, we then calculate the free data we will use when solving the CTS equations from the usual rela-

tions:

$$\tilde{\gamma}_{ij} = \gamma_{ij}^{(\text{sup})} \quad (14)$$

$$\dot{\tilde{\gamma}}^{ij} = -\tilde{\gamma}^{ik}\tilde{\gamma}^{jl} \left( \dot{\gamma}_{kl}^{(\text{sup})} - \frac{1}{3}\tilde{\gamma}^{mn}\dot{\gamma}_{mn}^{(\text{sup})}\tilde{\gamma}_{kl} \right) \quad (15)$$

$$\tilde{\alpha} = \alpha^{(\text{sup})} \quad (16)$$

$$K = \frac{1}{2\tilde{\alpha}} (2\partial_i \beta^{i(\text{sup})} + \dot{\tilde{\gamma}}^{ij}\tilde{\gamma}_{ij} + \tilde{\gamma}^{ij}\beta^{k(\text{sup})}\partial_k \tilde{\gamma}_{ij}). \quad (17)$$

For initial data with matter we use a similar method. We set  $\tilde{E}$  and  $\tilde{p}^i$  by superposing the energy and momentum density of the two objects (we do not consider situations where they would both be non-zero at the same point). For some cases (in particular for the ultrarelativistic boosts), we rescale the momentum density so that its magnitude with respect to the superposed metric  $\tilde{\gamma}_{ij}$  is equal to the magnitude of the original momentum density with respect to the metric of the isolated object ( $\gamma_{ij}^{(1)}$  or  $\gamma_{ij}^{(2)}$ ). This ensures that  $\tilde{E}^2$  and  $\tilde{p}^i \tilde{p}_i$  have the same ratio as the isolated objects. This is important since the choice of conformal scaling of the energy  $\tilde{E} = E\Psi^8$  was designed to ensure that if the conformal quantities satisfy the dominant energy condition,  $\sqrt{\tilde{\gamma}_{ij}\tilde{p}^i\tilde{p}^j} \leq \tilde{E}$ , then so will the rescaled quantities following the solution of the constraints.

### C. Regularizing black hole solutions

In cases where black holes are a part of the physical system, the divergences at the black hole’s singularity must be addressed. As discussed in the introduction, there are several ways to deal with this issue in the initial data problem; the approach we take here is to explicitly modify the metric of an isolated (prior to superposition) black hole solution inside the horizon to take a prescribed, regular form. The regularized region will not in general satisfy the vacuum constraint equations, and to avoid a singular conformal factor and shift vector components when solving the constraints with such background data, we introduce unphysical energy-momentum in the union of black hole interiors so that these regions automatically satisfy the constraints, albeit with the unphysical interior matter source.

We start with a single, unboosted spinning black hole spacetime in horizon penetrating coordinates (for the results described here we use the harmonic form of Kerr derived in [82], though we have also tried it using Kerr-Schild coordinates without difficulty), so that the only divergences in the metric components are well within the horizon. We then choose a surface that encloses the singular region, yet is strictly inside of the event horizon. The interior of this surface we call the *regularization region*. Outside the regularization region we do not modify the metric. Inside, there are many conceivable ways to alter the metric to eliminate the divergences. The simple

approach we take is to promote the black hole mass  $M$  and spin  $a$  constants to functions of space, and smoothly decrease them from their bare values at the regularization surface to zero at some surface interior to this.

Specifically, we introduce a regularization function

$$f_{\text{reg}}(x) = \begin{cases} 1 & x > 1 \\ x^3(6x^2 - 15x + 10) & 1 > x > 0 \\ 0 & 0 > x \end{cases} \quad (18)$$

chosen to be twice continuously differentiable so that the consequent unphysical energy is well-behaved. We use a Cartesian grid<sup>1</sup> and define  $r^{(E)}(x, y, z) = \sqrt{x^2 + y^2 + z^2}$  as the Euclidean radius for a point with coordinates  $x, y, z$ . We then replace the mass  $M$  and the spin parameter  $a$  with  $\xi(x, y, z)M$  and  $\xi(x, y, z)a$  respectively in all the metric components, where

$$\xi(x, y, z) = f_{\text{reg}}\left(\frac{(r^{(E)}(x, y, z)/r_+^{(E)}(x, y, z)) - q_{\text{in}}}{q_{\text{out}} - q_{\text{in}}}\right), \quad (19)$$

$r_+^{(E)}(x, y, z)$  is the Euclidean radius for the point on the event horizon at the same angular direction as  $(x, y, z)$ ,  $q_{\text{out}}$  defines the outer surface of the regularization region, and  $q_{\text{in}}$  the inner surface inside of which the metric is Minkowski, with  $1 > q_{\text{out}} > q_{\text{in}} > 0$ . The shape of the regularization region, namely a shrunken form of the interior of the event horizon, was motivated by the similar volume excised during evolution (though that is based on the apparent horizon, and the excision surface is a best-fit ellipsoid rather than the exact shape of the apparent horizon). The particular values of  $q_{\text{out}}$  and  $q_{\text{in}}$  are not too important (i.e., give essentially the same solutions), the only practical requirements being that  $q_{\text{out}}$  represents a surface within the excision surface we will use during evolution, and that  $q_{\text{in}}$  not be too close to  $q_{\text{out}}$ , otherwise excessive resolution is needed to resolve the transition.

Once we have an everywhere-regular metric, we superpose it with any other COs to construct the free data as described in Sec. II B. We then compute the unphysical energy and momentum we will add to the regularization regions simply by evaluating (4) and (5) with the background, superposed data:

$$E_{\text{unphys}} \equiv \frac{1}{16\pi}(R + K^2 + K_{ij}K^{ij})^{(\text{sup})} \quad (20)$$

$$p_{\text{unphys}}^i \equiv \frac{1}{8\pi}(D_j K^{ij} - D^i K)^{(\text{sup})}. \quad (21)$$

$E_{\text{unphys}}$  and  $p_{\text{unphys}}^i$  are then added to  $\tilde{E}$  and  $\tilde{p}^i$  within the

regularization regions<sup>2</sup>, and we can then solve the CTS equations as usual without any additional special treatment of these regions. During evolution, we choose black hole excision surfaces that entirely contain the regularization regions and unphysical matter. Thus, one can think of the unphysical matter as serving as a proxy for what would otherwise be boundary conditions for  $\Psi$  and  $\beta^i$  on excision surfaces. Given a solution to the constraints with regularized interiors it is trivial to read off what the equivalent (Dirichlet) boundary conditions would have been, though the inverse problem of mapping some set of desired boundary conditions to interior sources is less trivial, and likely not well-posed in general.

## D. Fluid Solutions

For the applications with (physical) matter considered here we use Tolman-Oppenheimer-Volkov (TOV) star solutions in isotropic coordinates to construct the metric free data quantities as well as  $\tilde{E}$  and  $\tilde{p}^i$ . Such solutions are derived by assuming a relationship between the pressure and density  $P(\rho)$ , e.g. as given by a polytropic condition. Once the constraint equations have been solved and  $E$  and  $p^i$  found, we determine the new density and pressure profiles using this same relationship and solving the equation

$$(E + P(\rho))(E - \rho) - p_i p^i = 0 \quad (22)$$

for  $\rho$ , which follows directly from the expressions for the energy and momentum density of a perfect fluid. For the applications considered here, we do not explicitly impose any additional constraints on the fluid quantities (e.g. that the fluid be in hydrostatic equilibrium). We leave that to future extensions.

## E. Multigrid elliptic solver

In order to numerically solve the CTS equations we discretize (8) and (9) using standard second-order finite difference operators and solve them using a full approximation storage implementation of the multigrid algorithm with Adaptive Mesh Refinement (AMR) as described in [83]. A multigrid algorithm is characterized by a smoothing operation, and a choice of restriction and prolongation operators. We use Newton-Gauss-Seidel relaxation for smoothing, and half-weight restriction and linear interpolation for the restriction and prolongation operators, respectively. These latter operators require special treatment on mesh refinement boundaries which we outline in the Appendix. Unlike in the evolution

<sup>1</sup> Note that in the harmonic coordinates of [82] only the region with  $r_K > M$  is represented on the Cartesian grid  $r \geq 0$ , where  $r_K$  is the radial coordinate of the the metric in ingoing null Kerr form. Hence the physical singularity is not on the grid, however, the metric components are discontinuous at  $x = y = z = 0$  ( $r_K = M$ ), hence regularization is still required.

<sup>2</sup> It is also possible to calculate the unphysical energy-momentum before the superposition, and add the free data  $E$  and  $\tilde{p}$  afterwards; either approach gives similar results.



code, we do not use a compactified coordinate system extending to spatial infinity, rather the initial data numerical grid extends to a large but finite radius. At the outer boundaries we impose boundary conditions that  $\Psi = 1$  and  $\beta^i = \beta^{i(\text{sup})}$ . Any points outside of this domain on the evolution grid are initialized via extrapolation, assuming a leading order  $1/r$  approach to an asymptotically-flat spacetime.

For some applications we wish to solve for initial data with axisymmetry. In order to efficiently solve the constraint equations in these situations we have implemented a modified version of the Cartoon method [84] similar to that used in [85]. Letting the  $y$ -axis be the axis of symmetry, we restrict our computational domain to a subset of the half plane  $(x, y) \in (-\infty, \infty) \times [0, \infty)$ . We use the existence of an axisymmetric Killing vector to express derivatives in the  $z$  direction in terms of derivatives in the  $x$  and  $y$  directions. On the  $y$ -axis we impose regularity which gives the following conditions for the constrained variables:  $\partial_y \Psi = 0$  and  $\partial_y \beta^x = \partial_y \beta^y = \beta^z = 0$ .

### III. APPLICATIONS

#### A. Quasi-circular binary black holes

As a first application of our technique, we generate and evolve ID for the (approximate) quasi-circular inspiral of two non-spinning, equal-mass black holes. Our present method for providing free data is not designed to easily give initial data for quasi-circular inspiral (though presumably with sufficient fine-tuning of the boost vectors this could be achieved), and this basic example is mainly to provide a relatively low eccentricity binary, a couple of orbits before merger, for comparison to past studies. Specifically, we are interested in seeing how the bare, input parameters of the black holes changing following solution of the constraints, and how much “spurious” gravitational radiation is present in the initial data.

For the initial data, we use free data set by superposing two boosted non-spinning equal mass black holes at a coordinate separation of  $10M$ , where  $M$  is the sum of the isolated black hole masses (which in general will be different from the irreducible masses of the black holes once the constraint equations are solved). The black holes are given purely tangential boost velocities chosen so that, when evolved, the black holes undergo a few orbits with monotonically decreasing proper separation. The initial data grid extends to  $\pm 2048M$  in all three directions. For convergence studies of the initial data solver, we use three base grid sizes of  $33^3$ ,  $65^3$  and  $129^3$  and 12 levels of mesh refinement with identical grid structures in each case. As expected, the conformal factor and shift vector exhibit second-order convergence as shown in Figs. 1 and 2, as does the residual of (4) and (5). For evolution, we use the highest resolution initial data. The ID is evolved using the generalized harmonic formulation of the field equations, choosing harmonic coordinates at

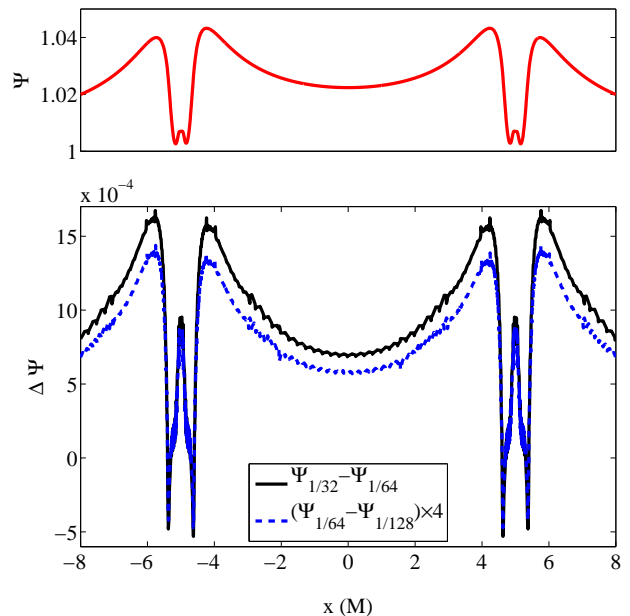


FIG. 1: The conformal factor  $\Psi$  from BH-BH ID. Upper:  $\Psi$  on the  $x$ -axis which lies on the orbital plane and goes through the centers of the black holes. Lower: Differences in  $\Psi$  with resolution on the  $x$ -axis, scaled assuming second-order convergence.

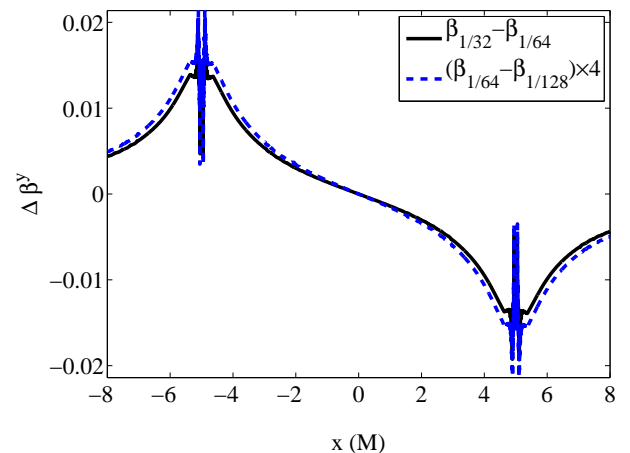


FIG. 2: Differences in the shift component  $\beta^y$  with resolution on the  $x$ -axis from BH-BH ID, scaled assuming second-order convergence.

$t = 0$  and transitioning to a damped harmonic gauge as described in [86]. The eccentricity is estimated to be  $e \approx 0.05$  based on the evolution of the coordinate distance between the centers of the apparent horizons as shown in Fig. 3. Though the orbital eccentricity could presumably be reduced further by tuning the initial velocities using methods such as the one proposed in [87], we did not attempt to do so for this basic comparison.

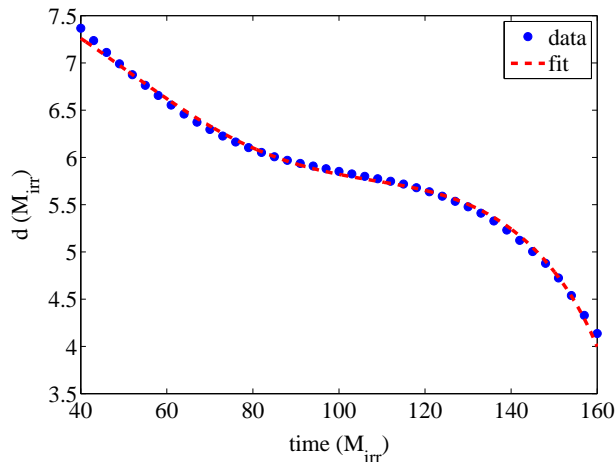


FIG. 3: Coordinate separation of the centers of the two black holes fitted to a function  $(A - B(t - t_0))^{1/4} + C \cos(\omega(t - t_0) + \phi)$ . This function combines the decaying orbit due to quadrupole radiation with the effects of eccentricity, given by  $e = C/d(t = t_0) \approx 0.05$ . Due to early-time gauge effects (a transition from harmonic to damped harmonic gauge) we exclude the first  $t = 40M_{\text{irr}}$  from the fit.

Because of corrections from solving the constraints, the sum of the masses of the isolated black holes whose space-times we superpose  $M$  is different from the sum of irreducible masses computed from their apparent horizons at the beginning of the evolution  $M_{\text{irr}}$ . For this particular case  $M_{\text{irr}}/M = 1.21$ . The ID is constructed using free data with non-spinning black holes, and the initial spin calculated from the apparent horizons is zero to within truncation error ( $|S/M_{\text{BH}}^2| < 6 \times 10^{-3}$ ). The ratio of the irreducible mass of the final black hole after the merger to sum of the irreducible masses of the initial black holes is  $M_{\text{irr},f}/M_{\text{irr}} = 0.885$ , and the dimensionless spin parameter of the final black hole is  $a_f/M_f = 0.678$ . Both of these values are in good agreement (considering the mild initial eccentricity here) with the high accuracy results of 0.88433 and 0.68646, respectively, from [88]. In Fig. 4 we show the gravitational waves from the BH-BH merger. The initial spurious part of the signal is of comparable magnitude to other ID approaches that do not attempt to include gravitational waves from the prior inspiral; see for example [70].

### B. Eccentric compact object mergers

As another application of this technique, we consider constructing initial data describing a dynamical capture BH-NS binary. We set the free data using a boosted harmonic black hole solution and a neutron star with the HB equation of state [89]. Let  $M$  be the sum of the masses of the isolated black hole and neutron star. We construct initial data for a 4:1 BH-NS binary by setting the boost

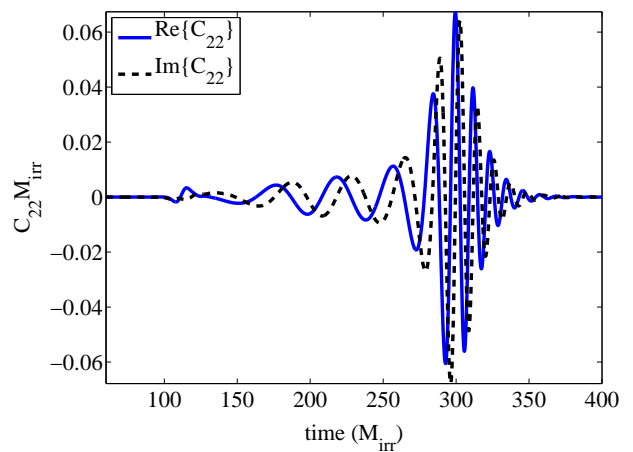


FIG. 4: The real and imaginary components of the  $l = 2$ ,  $m = 2$  spin-weight  $-2$  spherical-harmonic of  $r\Psi_4$  extracted at a radius of  $105M$ . Time is measured from the beginning of the simulation.

velocities to correspond to a Newtonian orbit with eccentricity  $e = 1$  and periaapse distance  $r_p = 5M$  at various initial separations  $d$ . We keep the mass and spin that we use for the black hole component of the free data fixed at  $0.8M$  and  $-0.4M$ , respectively, (where the negative sign indicates that the spin is retrograde with respect to the orbital angular momentum) and the mass of the neutron star component of the free data fixed at  $0.2M$ . The spin and masses will receive corrections from solving the constraint equations and with decreasing  $d$  these will differ more and more from the input parameters of the free data. The input parameters can of course be tuned to achieve desired values in the final solution. However, since here we are mainly interested in quantifying this difference, we keep them fixed. We use a grid extending from  $-1600M$  to  $1600M$  in each dimension where the base level is covered by  $257^3$  points and there are 9 additional levels of mesh refinement, each with a refinement ratio of two. We solve for data with initial separations  $d/M = 15, 25$ , and  $50$ . In Table I we show the maximum difference of the conformal factor from unity as well as the actual ADM (Arnowitt-Deser-Misner) mass, black hole mass and spin, neutron star rest-mass, and induced neutron star density oscillations for these three different separations. We can see that even at a separation of  $15M$  the difference between input and final parameters is small — at the level of a few percent. At such separations, however, the oscillations induced in the neutron star by the initial setup become large. This problem could be remedied by adding additional constraints to the matter, for example requiring it to satisfy an equilibrium version of the Euler equations.

We evolve the initial data past merger using the same methods, gauge, and three different resolutions as in [15]. Unless otherwise stated all quantities are from the high

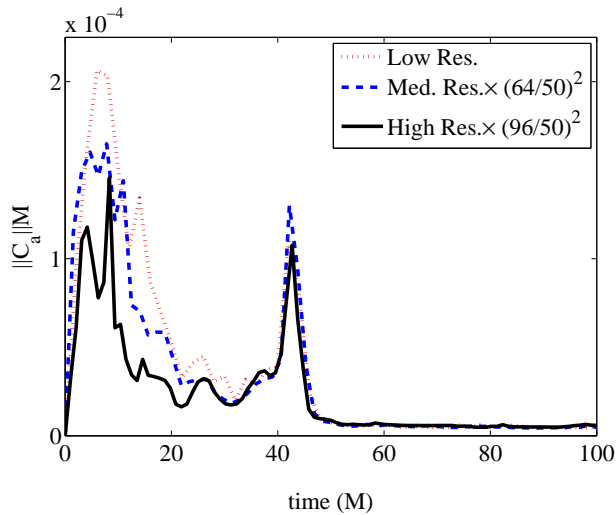


FIG. 5: The  $L^2$ -norm of the constraint violation,  $C_a \equiv H_a - \square x_a$ , in units of  $1/M$  for the  $d = 15M$  BH-NS merger in the  $100M \times 100M$ -region around the center of mass in the equatorial plane (i.e.  $\sqrt{\int \|C_a\|^2 d^2x} / \int d^2x$ ). This is shown for low, medium, and high resolutions where the latter two are scaled assuming second-order convergence.

resolution runs. In Fig. 5 we show the norm of the constraints throughout the evolution of the  $d = 15M$  ID at the different resolutions. The single highest, resolution ID is used for all evolution runs, so the fact evolution constraints are converging to zero indicates that the truncation error of the ID is at least as small as that of the highest resolution evolution. In Fig. 6 we plot the amplitude of the gravitational waves measured from the three different evolutions to show the amount of spurious gravitational radiation this method of constructing ID introduces. The level of spurious gravitational radiation decreases with increasing separation and in all three cases is small — an order of magnitude or more below the physical signal of interest. After the passage of the spurious gravitational radiation, the gravitational wave signal from all three initial separations is approximately the same, though there are small differences due to the changes in parameters indicated in Table I, and because we are starting the systems along different points of a Newtonian trajectory.

### C. Ultrarelativistic initial data

As a final application, we consider the problem of specifying ID for ultrarelativistic collisions. The study of the collision of objects where kinetic energy dominates the dynamics of the spacetime is of considerable interest to super-Planck scale particle collisions, as arguments suggest classical Einstein gravity will be adequate to describe the process [90–92]. The hoop con-

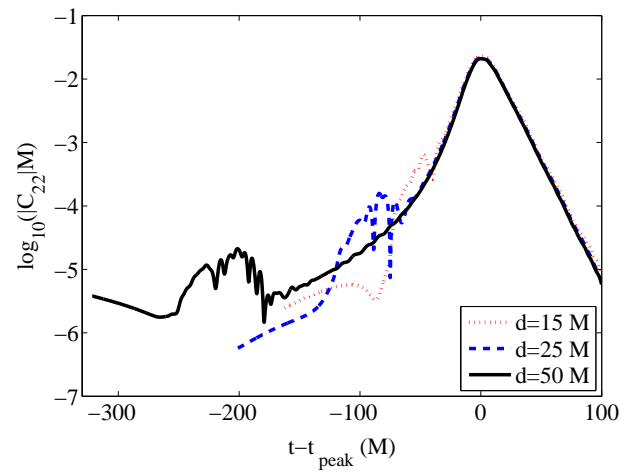


FIG. 6: The log of the magnitude of the  $l = 2$ ,  $m = 2$  spin-weight  $-2$  spherical harmonic of  $r\Psi_4$  for BH-NS simulations with different initial separations  $d$ . The value of  $\Psi_4$  was extracted on a sphere of radius  $100M$  and is shown starting at the beginning of the simulation and continuing past merger. The waveforms have been aligned so that the peaks occurs at time 0.

jecture [93] predicts that the generic outcome of a sufficiently ultrarelativistic collision will be black hole formation, and this, together with suggestions of a TeV Planck scale [94, 95], imply that, if such a scenario describes nature, the Large Hadron Collider (LHC) or cosmic ray collisions with Earth could produce black holes [96–98]. Though to date no signs of black hole production have been observed [99, 100], the nature of the kinetic energy dominated regime in general relativity is of interest in its own right, and has largely been unexplored.

Initial data describing such systems will be far from equilibrium and one cannot assume that the solution is time-symmetric or quasi-static. It is instructive to recall the Aichelburg-Sexl [101] solution describing a gravitational shockwave. The solution can be obtained from a boosted Schwarzschild solution by simultaneously taking the mass to zero and the boost parameter to infinity, while keeping their product constant and finite. Two such oppositely boosted solutions can be superposed to obtain a new solution that is valid up until collision. Though it is not clear how applicable this is to the non-limiting case, this suggests that superposition may be a good approximation to describing such spacetimes.

Here we consider the specific example of the setup for a head-on collision of two fluid star solutions. We use the method described in Sec. IIB to construct free data from two  $\Gamma = 2$  polytropic TOV star solutions that have unboosted mass  $M_*$  and a compactness (ratio of mass-to-radius) of  $C = 0.01$ . The stars are boosted towards each other with boost factor  $\gamma = 10$ . We consider a sequence of solutions at various initial coordinate separations  $d$ . We take advantage of the axisymmetry of the problem and

$d/M$	$\max( \Psi - 1 )$	$M_0/M_{0,\infty}$	$M_{\text{BH}}/M$	$a_{\text{BH}}/M$	$M_{\text{ADM}}/M$	$\rho_{\text{oscill.}} (\%)$
15	0.0155	1.077	0.832	-0.398	1.051	14.3
25	0.0092	1.049	0.818	-0.402	1.030	9.0
50	0.0046	1.028	0.808	-0.399	1.017	4.5

TABLE I: Characteristics of BH-NS initial data with Newtonian orbital parameters  $r_p = 5M$  and  $e = 1$  with three initial coordinate separations  $d$ . Here  $\max(|\Psi - 1|)$  is the maximum deviation over the entire domain of the conformal factor from the background free-data value of unity,  $M_0/M_{0,\infty}$  is the rest-mass of the neutron star compared to its isolated rest-mass,  $M_{\text{BH}}/M$  and  $a_{\text{BH}}/M$  are the black hole mass and spin parameters measured from the apparent horizon relative to the initial total mass  $M$  of the free data,  $M_{\text{ADM}}/M$  is the relative ADM mass of the solution, and  $\rho_{\text{oscill.}}$  is the relative magnitude of the oscillation in time of the maximum rest-mass density of the neutron star induced by the ID construction.

use  $[-2000M, 2000M] \times [0, 2000M]$  where  $M \equiv 2\gamma M_*$  as our computational domain. The base level is covered by  $1025 \times 513$  points and there are 9 additional levels of mesh refinement. To test convergence we also consider two lower resolutions with grid spacing 2 and 4/3 times as coarse.

Using the method for specifying free data described in Sec. II B, as  $d \rightarrow \infty$  we expect the corrections from solving the constraints will go to zero:  $\Psi \rightarrow 1$ , the magnitude of the coordinate velocities of the stars  $|v|$  will approach  $\sqrt{1 - \gamma^{-2}}$ , the ADM mass  $M_{\text{ADM}}$  will approach  $M$ , and the total rest-mass  $M_0$  will approach the sum of the rest-masses of the isolated stars  $M_{0,\infty}$ . In Fig. 7 we show how all these quantities change with coordinate separation. We can see that it is possible to solve for ID where the stars are quite close together, though the corrections become large, and in particular the ADM mass decreases quite significantly.

To give an indication of the numerical errors on these quantities we can compare the values obtained at the highest resolution to the Richardson extrapolated values using all the three resolutions. For example, for the smallest separation  $d = 1.56M$ , we have  $\max(|\Psi - 1|) = 0.05326$  (0.05325) and  $\max|v| = 0.530149$  (0.530153) where the values in parentheses are the Richardson extrapolated quantities (which are consistent with approximately second-order convergence).

We can compare the above method of constructing free data for this case to a conformally flat method. Specifically, we set all the metric free data quantities to their flatspace values, and set  $\tilde{E}$  and  $\tilde{p}^i$  for each star to a special-relativistically boosted density and pressure profile taken from the TOV solution. In Fig. 8 we show the same quantities as in Fig. 7 but using this conformally flat method. In this case the corrections from solving the constraints will not go to zero with infinite separation since all the non-trivial geometry is coming from the conformal factor. Hence the energy-momentum will be substantially rescaled at any separation. Also in contrast to the first method, the maximum of  $|\Psi - 1|$  occurs for  $\Psi > 1$  instead of  $\Psi < 1$ , which means  $E$  and  $p^i$  will be smaller than their conformal counterparts. With conformally flat ID it is also possible to solve for stars close together though, as in the previous method, the ADM

mass decreases steeply. It should also be noted that because of the large shift vector obtained with the second method, the coordinate velocity is substantially greater than one, which may make it more challenging to numerically evolve.

A full characterization of this ultrarelativistic collision ID will require evolution, which we will present in upcoming work [102].

#### IV. CONCLUSIONS

We have outlined a general method for constructing initial data based on superposition and the CTS formulation of the constraint equations, and demonstrated the method with some example solutions. Though there are numerous existing applications of the CTS method, and superposition has been proposed before, some of the novel aspects of the work presented here include adding neutron stars to the prescription, regularizing the interiors of black holes with (unphysical) matter sources, and applying it to regimes not yet studied before, namely initial data for high-eccentricity binary mergers and ultrarelativistic collisions. For astrophysically relevant binaries we find that superposition of single, isolated compact object solutions works well in the sense that non-linear correction from solving the constraints are relatively small for larger initial separations, implying that superposition is a good start to attain more astrophysically realistic initial data (for example, by adding prior gravitational wave information as in [70] to the superposed background data for quasi-circular or low eccentricity inspirals). Including neutron stars, we find that the superposition effectively induces oscillations in the stars. This again is small for large separations and hence a good approximation to dynamical capture binaries. However, practical application to low eccentricity inspirals will likely require that the CTS equations be supplemented with some form of quasi-equilibrium equations for the hydrodynamics (as in many existing ID methods, for example [54, 59, 72]).

For the ultrarelativistic boost examples we are able to obtain solutions to the CTS equations with superposed and conformally flat data well into the kinetic energy



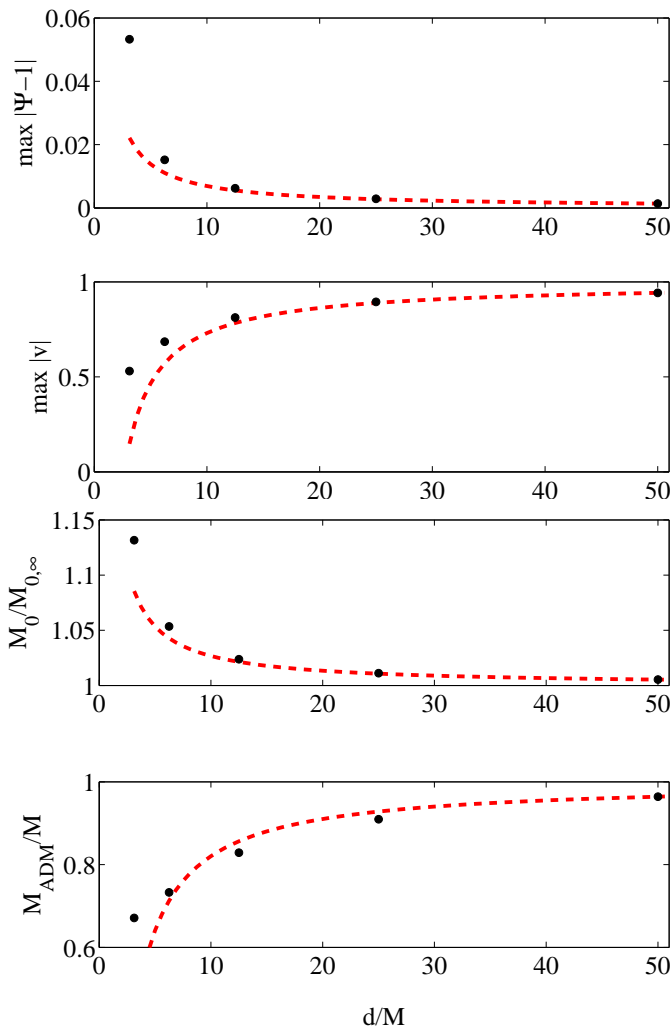


FIG. 7: Various quantities from ultrarelativistic collision ID with  $\gamma = 10$  made using the superposition method for constructing free data. From top to bottom the quantities shown are the maximum (over the entire domain) difference of the conformal factor from unity, the maximum coordinate velocity of the fluid, the total rest-mass, and the ADM mass. All quantities are shown as a function of  $d$ , the coordinate separation between the two stars. For all these cases the maximum of  $|\Psi - 1|$  occurs for values of  $\Psi$  that are less than unity. One might expect these quantities to approach their infinite separation limits as  $1/d$  for large  $d$ ; the dotted lines show such  $1/d$  curves for each quantity matched to the  $d/M = 50$  point.

dominated regime ( $\gamma = 10$ ) for sufficiently large initial separations. At smaller separations we are still able to obtain solutions. However, for these initial data sets the corrections to the metric and fluid properties become large, and it is less clear how to separate the total energy of the spacetime into kinetic energy, rest-mass energy, etc. This will require evolution to resolve, and we leave that to future work. Nevertheless, given that there are few results on the uniqueness and existence of solutions

to the conformal constraint equations beyond constant mean curvature slicing [103] (and in some cases, such as the extended CTS equations [104] there are known examples of non-uniqueness [105]), it is interesting that we are able to obtain solutions in this highly non-linear regime.

### Acknowledgments

We thank Geoffrey Lovelace and Sean McWilliams for useful conversations. We thank Hans Bantilan and Theodor Brasoveanu for working on a prototype of the software used here. This research was supported by NSF grant PHY-0745779 and the Alfred P. Sloan Foundation (FP). Simulations were run on the Woodhen and Orbital clusters at Princeton University as well as using XSEDE resources provided by NICS under Grant No. TG-PHY100053.

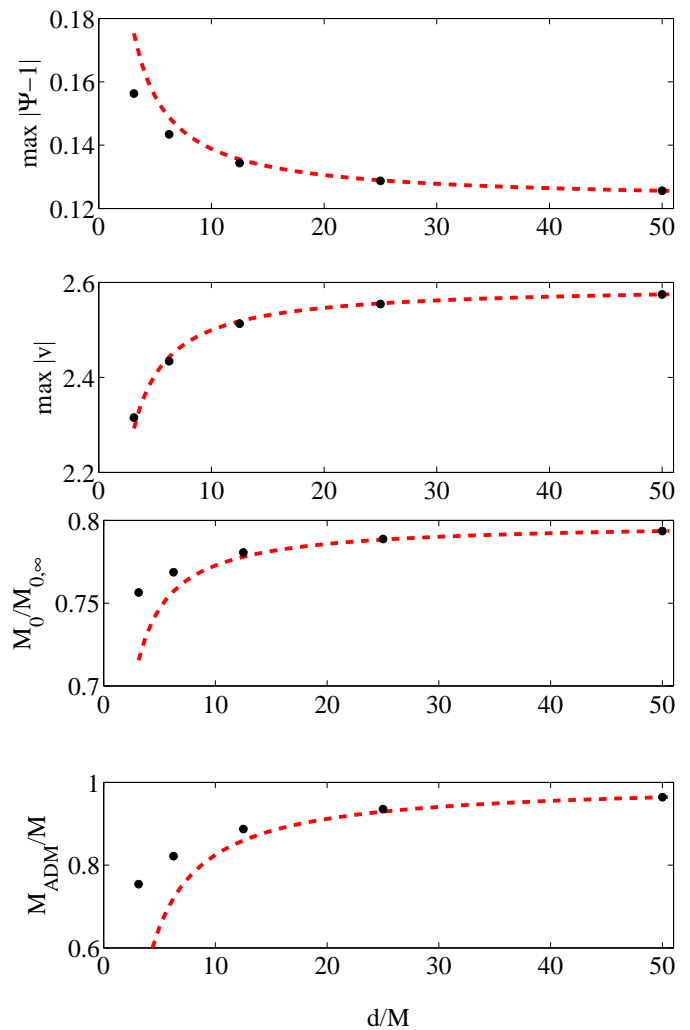


FIG. 8: Same as Fig. 7 but with conformally flat data. For all these cases the maximum of  $|\Psi - 1|$  occurs for values of  $\Psi$  that are greater than unity.

## Appendix: Multigrid AMR interpolation

A multigrid algorithm requires a restriction operator to inject quantities from finer to coarser grids as well as a prolongation operator to interpolate corrections from coarser grids to finer grids (see e.g. [106]). For our multigrid algorithm we use half-weight restriction as our restriction operator. In three dimensions half-weight restriction can be written as

$$f_{\text{HW}} = f_{i,j,k} + \frac{1}{12}(\Delta f_{xx} + \Delta f_{yy} + \Delta f_{zz}) \quad (\text{A.1})$$

where

$$\Delta_{xx}f = f_{i+1,j,k} - 2f_{i,j,k} + f_{i-1,j,k} \quad (\text{A.2})$$

and similarly for the  $y$  and  $z$  directions. Note that  $\Delta_{xx}f$  divided by  $h^2$  (where  $h$  is the grid spacing) is a second-order approximation for  $\partial_x^2 f$ . On AMR boundaries where

the full stencil is not available we must modify the above expression. For example on a negative  $x$ -boundary we replace  $\Delta_{xx}f$  by a right-handed second derivative stencil

$$\Delta_{xx}f = 2f_{i,j,k} - 5f_{i-1,j,k} + 4f_{i-2,j,k} - f_{i-3,j,k} \quad (\text{A.3})$$

and so on for the other directions. This ensures not only that  $f_{\text{HW}}$  is a second-order representation of  $f$ , but also that  $f_{\text{HW}}$  is smooth to  $O(h^4)$  on AMR boundaries. Hence if second derivatives of  $f_{\text{HW}}$  are computed including restricted boundary points in the stencil the error will be  $O(h^2)$ .

We use linear interpolation as our prolongation operator. However, after applying a correction from a coarse grid, we reset the values on the AMR boundaries of the fine grid for the points that do not exist on the coarse level with fourth-order interpolation using those points that do. We found this higher order interpolation to be beneficial as we do not relax the points on the boundary.

- 
- [1] A. Abramovici et al. Ligo: The laser interferometer gravitational wave observatory. *Science*, 256:325, 1992.
  - [2] B. Caron et al. The virgo interferometer. *Class. and Quant. Grav.*, 14:1461, 1997.
  - [3] H. Lück et al. The geo-600 project. *Class. and Quant. Grav.*, 15:1471, 1997.
  - [4] Kentaro Somiya. Detector configuration of KAGRA - the Japanese cryogenic gravitational-wave detector. *Class.Quant.Grav.*, 29:124007, 2012.
  - [5] B. Sathyaprakash, M. Abernathy, F. Acernese, P. Ajith, B. Allen, et al. Scientific Objectives of Einstein Telescope. *Class.Quant.Grav.*, 29:124013, 2012.
  - [6] Harald P Pfeiffer. Numerical simulations of compact object binaries. *Classical and Quantum Gravity*, 29(12):124004, 2012.
  - [7] Sean T McWilliams. The status of black-hole binary merger simulations with numerical relativity. *Classical and Quantum Gravity*, 28(13):134001, 2011.
  - [8] Frans Pretorius. Binary Black Hole Coalescence. 2007.
  - [9] Joan Centrella, John G. Baker, Bernard J. Kelly, and James R. van Meter. Black-hole binaries, gravitational waves, and numerical relativity. *Rev.Mod.Phys.*, 82:3069, 2010.
  - [10] Joshua A. Faber and Frederic A. Rasio. Binary neutron star mergers. *Living Reviews in Relativity*, 15(8), 2012.
  - [11] Masaru Shibata and Keisuke Taniguchi. Coalescence of black hole-neutron star binaries. *Living Reviews in Relativity*, 14(6), 2011.
  - [12] Matthew D. Duez. Numerical relativity confronts compact neutron star binaries: a review and status report. *Class.Quant.Grav.*, 27:114002, 2010.
  - [13] Branson C. Stephens, William E. East, and Frans Pretorius. Eccentric Black Hole-Neutron Star Mergers. *Astrophys.J.*, 737:L5, 2011.
  - [14] Roman Gold, Sebastiano Bernuzzi, Marcus Thierfelder, Bernd Bruegmann, and Frans Pretorius. Eccentric binary neutron star mergers. 2011.
  - [15] William E. East, Frans Pretorius, and Branson C. Stephens. Eccentric black hole-neutron star mergers: Effects of black hole spin and equation of state. *Phys. Rev. D*, 85:124009, Jun 2012.
  - [16] Christian D. Ott. The Gravitational Wave Signature of Core-Collapse Supernovae. *Class.Quant.Grav.*, 26:063001, 2009.
  - [17] Chris L. Fryer and Kimberly C.B. New. Gravitational waves from gravitational collapse. *Living Reviews in Relativity*, 14(1), 2011.
  - [18] Jos A. Font. Numerical hydrodynamics and magnetohydrodynamics in general relativity. *Living Reviews in Relativity*, 11(7), 2008.
  - [19] Beverly K. Berger. Numerical approaches to spacetime singularities. *Living Reviews in Relativity*, 5(1), 2002.
  - [20] David Garrison. Numerical Relativity as a tool for studying the Early Universe. 2012.
  - [21] V. et al. Cardoso. NR/HEP: roadmap for the future. *ArXiv e-prints*, January 2012.
  - [22] Carsten Gundlach and Jose M. Martin-Garcia. Critical phenomena in gravitational collapse. *Living Reviews in Relativity*, 10(5), 2007.
  - [23] Ulrich Sperhake, Vitor Cardoso, Frans Pretorius, Emanuele Berti, and Jose A. Gonzalez. The High-energy collision of two black holes. *Phys.Rev.Lett.*, 101:161101, 2008.
  - [24] Masaru Shibata, Hirotada Okawa, and Tetsuro Yamamoto. High-velocity collision of two black holes. *Phys.Rev.*, D78:101501, 2008.
  - [25] Matthew W. Choptuik and Frans Pretorius. Ultra Relativistic Particle Collisions. *Phys.Rev.Lett.*, 104:111101, 2010.
  - [26] Hirotada Okawa, Ken-ichi Nakao, and Masaru Shibata. Is super-Planckian physics visible? - Scattering of black holes in 5 dimensions. *Phys.Rev.*, D83:121501, 2011.
  - [27] Helvi Witek, Vitor Cardoso, Leonardo Gualtieri, Carlos Herdeiro, Ulrich Sperhake, et al. Head-on collisions of unequal mass black holes in D=5 dimensions. *Phys.Rev.*, D83:044017, 2011.

- [28] Paul M. Chesler and Laurence G. Yaffe. Horizon formation and far-from-equilibrium isotropization in supersymmetric Yang-Mills plasma. *Phys.Rev.Lett.*, 102:211601, 2009.
- [29] Paul M. Chesler and Laurence G. Yaffe. Holography and colliding gravitational shock waves in asymptotically AdS<sub>5</sub> spacetime. *Phys.Rev.Lett.*, 106:021601, 2011.
- [30] Paul M. Chesler and Derek Teaney. Dynamical Hawking Radiation and Holographic Thermalization. 2011.
- [31] Hans Bantilan, Frans Pretorius, and Steven S. Gubser. Simulation of Asymptotically AdS<sub>5</sub> Spacetimes with a Generalized Harmonic Evolution Scheme. *Phys.Rev.*, D85:084038, 2012.
- [32] Alex Buchel, Luis Lehner, and Robert C. Myers. Thermal quenches in  $N=2^*$  plasmas. 2012.
- [33] Toby Wiseman. Numerical construction of static and stationary black holes. 2011.
- [34] Masaru Shibata and Hirotaka Yoshino. Nonaxisymmetric instability of rapidly rotating black hole in five dimensions. *Phys.Rev.*, D81:021501, 2010.
- [35] Luis Lehner and Frans Pretorius. Black Strings, Low Viscosity Fluids, and Violation of Cosmic Censorship. *Phys.Rev.Lett.*, 105:101102, 2010.
- [36] Piotr Bizon and Andrzej Rostworowski. On weakly turbulent instability of anti-de Sitter space. *Phys.Rev.Lett.*, 107:031102, 2011.
- [37] James W. York. Conformal “thin-sandwich” data for the initial-value problem of general relativity. *Phys. Rev. Lett.*, 82:1350–1353, Feb 1999.
- [38] Gregory B. Cook. Initial data for numerical relativity. *Living Reviews in Relativity*, 3(5), 2000.
- [39] E.ourgoulhon. Construction of initial data for 3+1 numerical relativity. *Journal of Physics Conference Series*, 91(1):012001, November 2007.
- [40] J. W. York, Jr. *Initial data for collisions of black holes and other gravitational miscellany.*, pages 89–109. 1989.
- [41] H. P. Pfeiffer. The initial value problem in numerical relativity. *ArXiv General Relativity and Quantum Cosmology e-prints*, December 2004.
- [42] J. M. Bowen and J. W. York, Jr. Time-asymmetric initial data for black holes and black-hole collisions. *Phys. Rev. D*, 21:2047–2056, April 1980.
- [43] A. Garat and R. H. Price. Nonexistence of conformally flat slices of the Kerr spacetime. *Phys. Rev. D*, 61(12):124011, June 2000.
- [44] G. B. Cook and J. W. York, Jr. Apparent horizons for boosted or spinning black holes. *Phys. Rev. D*, 41:1077–1085, February 1990.
- [45] Gregory B. Cook. Corotating and irrotational binary black holes in quasicircular orbits. *Phys. Rev. D*, 65:084003, Mar 2002.
- [46] Ericourgoulhon, Philippe Grandclément, and Silvano Bonazzola. Binary black holes in circular orbits. i. a global spacetime approach. *Phys. Rev. D*, 65:044020, Jan 2002.
- [47] Philippe Grandclément, Ericourgoulhon, and Silvano Bonazzola. Binary black holes in circular orbits. ii. numerical methods and first results. *Phys. Rev. D*, 65:044021, Jan 2002.
- [48] P. Grandclément. Accurate and realistic initial data for black hole neutron star binaries. *Phys. Rev. D*, 74(12):124002, December 2006.
- [49] F. Foucart, L. E. Kidder, H. P. Pfeiffer, and S. A. Teukolsky. Initial data for black hole neutron star binaries: A flexible, high-accuracy spectral method. *Phys. Rev. D*, 77(12):124051, June 2008.
- [50] G. B. Cook, M. W. Choptuik, M. R. Dubal, S. Klasky, R. A. Matzner, and S. R. Oliveira. Three-dimensional initial data for the collision of two black holes. *Phys. Rev. D*, 47:1471–1490, February 1993.
- [51] Gregory B. Cook. Three-dimensional initial data for the collision of two black holes. 2: Quasicircular orbits for equal mass black holes. *Phys.Rev.*, D50:5025–5032, 1994.
- [52] J. R. Wilson, G. J. Mathews, and P. Marronetti. Relativistic numerical model for close neutron-star binaries. *Phys. Rev. D*, 54:1317–1331, July 1996.
- [53] T. W. Baumgarte, G. B. Cook, M. A. Scheel, S. L. Shapiro, and S. A. Teukolsky. Binary Neutron Stars in General Relativity: Quasiequilibrium Models. *Physical Review Letters*, 79:1182–1185, August 1997.
- [54] Silvano Bonazzola, Ericourgoulhon, and Jean-Alain Marck. A Relativistic formalism to compute quasiequilibrium configurations of nonsynchronized neutron star binaries. *Phys.Rev.*, D56:7740–7749, 1997.
- [55] Wolfgang Tichy and Bernd Bruegmann. Quasiequilibrium binary black hole sequences for puncture data derived from helical Killing vector conditions. *Phys.Rev.*, D69:024006, 2004.
- [56] Gregory B. Cook and Harald P. Pfeiffer. Excision boundary conditions for black hole initial data. *Phys.Rev.*, D70:104016, 2004.
- [57] Marcus Ansorg, Bernd Bruegmann, and Wolfgang Tichy. A Single-domain spectral method for black hole puncture data. *Phys.Rev.*, D70:064011, 2004.
- [58] Marcus Ansorg. A Double-domain spectral method for black hole excision data. *Phys.Rev.*, D72:024018, 2005.
- [59] M. Shibata, K. Uryū, and J. L. Friedman. Deriving formulations for numerical computation of binary neutron stars in quasicircular orbits. *Phys. Rev. D*, 70(4):044044, August 2004.
- [60] Keisuke Taniguchi, Thomas W. Baumgarte, Joshua A. Faber, and Stuart L. Shapiro. Quasiequilibrium sequences of black-hole neutron-star binaries in general relativity. *Phys. Rev. D*, 74:041502, Aug 2006.
- [61] G. Lovelace, R. Owen, H. P. Pfeiffer, and T. Chu. Binary-black-hole initial data with nearly extremal spins. *Phys. Rev. D*, 78(8):084017, October 2008.
- [62] Geoffrey Lovelace. Reducing spurious gravitational radiation in binary-black-hole simulations by using conformally curved initial data. *Classical and Quantum Gravity*, 26(11):114002, 2009.
- [63] Richard A. Matzner, Mijan F. Huq, and Deirdre Shoemaker. Initial data and coordinates for multiple black hole systems. *Phys. Rev. D*, 59:024015, Dec 1998.
- [64] Pedro Marronetti and Richard A. Matzner. Solving the initial value problem of two black holes. *Phys. Rev. Lett.*, 85:5500–5503, Dec 2000.
- [65] Yuk Tung Liu, Zachariah B. Etienne, and Stuart L. Shapiro. Evolution of near-extremal-spin black holes using the moving puncture technique. *Phys.Rev.*, D80:121503, 2009.
- [66] Wolfgang Tichy, Bernd Brüggmann, Manuela Campanelli, and Peter Diener. Binary black hole initial data for numerical general relativity based on post-newtonian data. *Phys. Rev. D*, 67:064008, Mar 2003.
- [67] Samaya Nissanke. Post-newtonian freely specifiable initial data for binary black holes in numerical relativity.

- Phys. Rev. D*, 73:124002, Jun 2006.
- [68] Nicolas Yunes, Wolfgang Tichy, Benjamin J. Owen, and Bernd Bruegmann. Binary black hole initial data from matched asymptotic expansions. *Phys.Rev.*, D74:104011, 2006.
  - [69] Nathan K. Johnson-McDaniel, Nicolas Yunes, Wolfgang Tichy, and Benjamin J. Owen. Conformally curved binary black hole initial data including tidal deformations and outgoing radiation. *Phys.Rev.*, D80:124039, 2009.
  - [70] G. Reifenberger and W. Tichy. Alternatives to standard puncture initial data for binary black hole evolution. *ArXiv e-prints*, May 2012.
  - [71] G. Lovelace, M. A. Scheel, and B. Szilágyi. Simulating merging binary black holes with nearly extremal spins. *Phys. Rev. D*, 83(2):024010, January 2011.
  - [72] M. Shibata, K. Uryū, and J. L. Friedman. Erratum: Deriving formulations for numerical computation of binary neutron stars in quasicircular orbits [ *Phys. Rev. D* 70, 044044 (2004)]. *Phys. Rev. D*, 70(12):129901, December 2004.
  - [73] Koji Uryu, Francois Limousin, John L. Friedman, Ericourgoulhon, and Masaru Shibata. Binary neutron stars in a waveless approximation. *Phys.Rev.Lett.*, 97:171101, 2006.
  - [74] K. Uryū, F. Limousin, J. L. Friedman, E.ourgoulhon, and M. Shibata. Nonconformally flat initial data for binary compact objects. *Phys. Rev. D*, 80(12):124004, December 2009.
  - [75] Gregory B. Cook and Harald P. Pfeiffer. Excision boundary conditions for black-hole initial data. *Phys. Rev. D*, 70:104016, Nov 2004.
  - [76] Jason D. Immerman and Thomas W. Baumgarte. Trumpet-puncture initial data for black holes. *Phys.Rev.*, D80:061501, 2009.
  - [77] Steven Brandt and Bernd Bruegmann. A Simple construction of initial data for multiple black holes. *Phys.Rev.Lett.*, 78:3606–3609, 1997.
  - [78] Thomas W. Baumgarte. An alternative approach to solving the Hamiltonian constraint. *Phys.Rev.*, D85:084013, 2012.
  - [79] David Brown, Olivier Sarbach, Erik Schnetter, Manuel Tiglio, Peter Diener, Ian Hawke, and Denis Pollney. Excision without excision. *Phys. Rev. D*, 76:081503, Oct 2007.
  - [80] David Brown, Peter Diener, Olivier Sarbach, Erik Schnetter, and Manuel Tiglio. Turduckening black holes: An analytical and computational study. *Phys. Rev. D*, 79:044023, Feb 2009.
  - [81] Pedro Marronetti, Mijan Huq, Pablo Laguna, Luis Lehner, Richard A. Matzner, et al. Approximate analytical solutions to the initial data problem of black hole binary systems. *Phys.Rev.*, D62:024017, 2000.
  - [82] Gregory B. Cook and Mark A. Scheel. Well behaved harmonic time slices of a charged, rotating, boosted black hole. *Phys.Rev.*, D56:4775–4781, 1997.
  - [83] Frans Pretorius and Matthew W. Choptuik. Adaptive mesh refinement for coupled elliptic-hyperbolic systems. *J.Comput.Phys.*, 218:246–274, 2006.
  - [84] M. Alcubierre, S. Brandt, B. Bruegmann, D. Holz, E. Seidel, R. Takahashi, and J. Thornburg. Symmetry without Symmetry: Numerical Simulation of Axisymmetric Systems using Cartesian Grids. *Int. J. Mod. Phys.*, D10:273–290, 2001.
  - [85] Frans Pretorius. Numerical relativity using a generalized harmonic decomposition. *Class.Quant.Grav.*, 22:425–452, 2005.
  - [86] William E. East, Frans Pretorius, and Branson C. Stephens. Hydrodynamics in full general relativity with conservative adaptive mesh refinement. *Phys. Rev. D*, 85:124010, Jun 2012.
  - [87] Harald P. Pfeiffer, Duncan A Brown, Lawrence E Kidder, Lee Lindblom, Geoffrey Lovelace, and Mark A Scheel. Reducing orbital eccentricity in binary black hole simulations. *Classical and Quantum Gravity*, 24(12):S59, 2007.
  - [88] M. A. Scheel, M. Boyle, T. Chu, L. E. Kidder, K. D. Matthews, and H. P. Pfeiffer. High-accuracy waveforms for binary black hole inspiral, merger, and ringdown. *Phys. Rev. D*, 79(2):024003, January 2009.
  - [89] J. S. Read, C. Markakis, M. Shibata, K. Uryū, J. D. E. Creighton, and J. L. Friedman. Measuring the neutron star equation of state with gravitational wave observations. *Phys. Rev. D*, 79(12):124033, 2009.
  - [90] G. 't Hooft. Graviton dominance in ultra-high-energy scattering. *Physics Letters B*, 198:61–63, November 1987.
  - [91] T. Banks and W. Fischler. A Model for High Energy Scattering in Quantum Gravity. *ArXiv High Energy Physics - Theory e-prints*, June 1999.
  - [92] E. Kohlprath and G. Veneziano. Black holes from high-energy beam-beam collisions. *Journal of High Energy Physics*, 6:57, June 2002.
  - [93] K. S. Thorne. In J. Klauder, editor, *Magic Without Magic: John Archibald Wheeler*, page 231, San Francisco, 1972. Freeman.
  - [94] N. Arkani-Hamed, S. Dimopoulos, and G. Dvali. The hierarchy problem and new dimensions at a millimeter. *Physics Letters B*, 429:263–272, June 1998.
  - [95] L. Randall and R. Sundrum. Large Mass Hierarchy from a Small Extra Dimension. *Physical Review Letters*, 83:3370–3373, October 1999.
  - [96] S. Dimopoulos and G. Landsberg. Black Holes at the Large Hadron Collider. *Physical Review Letters*, 87(16):161602, October 2001.
  - [97] S. B. Giddings and S. Thomas. High energy colliders as black hole factories: The end of short distance physics. *Phys. Rev. D*, 65(5):056010, March 2002.
  - [98] J. L. Feng and A. D. Shapere. Black Hole Production by Cosmic Rays. *Physical Review Letters*, 88(2):021303, January 2002.
  - [99] (Ed.) de los Heros, C. Proceedings of the First Workshop on Exotic Physics with Neutrino Telescopes, EPNT06. 2007.
  - [100] Serguei Chatrchyan et al. Search for microscopic black holes in pp collisions at  $\sqrt{s} = 7$  TeV. *JHEP*, 1204:061, 2012.
  - [101] P. C. Aichelburg and R. U. Sexl. On the Gravitational field of a massless particle. *Gen. Rel. Grav.*, 2:303–312, 1971.
  - [102] William E. East and Frans Pretorius. 2012. in prep.
  - [103] A. Rendall. Local and Global Existence Theorems for the Einstein Equations. *Living Reviews in Relativity*, 5:6, September 2002.
  - [104] Harald P. Pfeiffer and James W. York. Extrinsic curvature and the einstein constraints. *Phys. Rev. D*, 67:044022, Feb 2003.
  - [105] H. P. Pfeiffer and J. W. York. Uniqueness and Nonuniqueness in the Einstein Constraints. *Physical Re-*



- view Letters*, vol. 95, Issue 9, id. 091101, 95(9):091101, August 2005.
- [106] William H. Press, Saul A. Teukolsky, William T. Vetterling, and Brian P. Flannery. *Numerical Recipes: The Art of Scientific Computing*. Cambridge University Press, 3rd edition, 2007.